

## Noninteracting-band model for dielectric screening and local-field corrections in bcc transition metals: Application to paramagnetic chromium

Joginder Singh, Natthi Singh, and Satya Prakash

*Physics Department, Panjab University, Chandigarh-160014, India*

(Received 20 November 1974)

An isotropic-noninteracting-band model is constructed using the energy eigenvalues calculated by Gupta and Sinha along the three principal symmetry directions [100], [110], [111] and along the three off-symmetry directions [310], [311], and [221]. It is found that three  $d$  subbands and the  $s$  band are partially filled and two  $d$  subbands are completely filled. The numbers of electrons per atom are assigned to the partially filled  $d$  subbands in the ratio of the volume occupied by them. The contributions to the dielectric matrix  $\epsilon(\vec{q}+\vec{G}, \vec{q}+\vec{G}')$ , which arise because of the intraband and interband transitions, are evaluated explicitly using the free-electron approximation for the electrons in the  $s$  band, and a simple tight-binding scheme for the electrons in the  $d$  subbands. The diagonal part of the dielectric function is compared with the detailed calculations of Gupta and Sinha. The anisotropy of the dielectric function is found to be small. The nondiagonal part of the dielectric function, which gives rise to local-field corrections, is found to be larger than the diagonal part for large values of the wave vector.

### I. INTRODUCTION

The quantum-mechanical treatment of the frequency and the wave-number-dependent dielectric function was given by Nozières and Pines<sup>1</sup> and by Ehrenreich and Cohen.<sup>2</sup> These authors have given the explicit expression for the longitudinal component of the dielectric tensor, and evaluated in the free-electron approximation. Adler<sup>3</sup> extended the formalism for the full dielectric tensor and also included the local-field effects which he evaluated for the cubic insulating solid. The formal microscopic theory of dielectric screening was also studied by Sham<sup>4</sup> for transition-metal compounds and by Shimizu and Hayashi<sup>5</sup> for transition metals.

Earlier, one of us studied the diagonal part of the dielectric matrix for the fcc transition-metal paramagnetic nickel in the noninteracting-band scheme for  $s$  and  $d$  conduction electrons<sup>6</sup> (hereafter this paper is referred to as I) and used this dielectric function to calculate the phonon frequencies.<sup>7</sup> The scheme was further extended for noble metals.<sup>8</sup> Very recently, we studied the dielectric function for ferromagnetic nickel<sup>9</sup> (hereafter this paper is referred to as II), in the noninteracting-spin band model where the calculations are also extended for the nondiagonal part of the dielectric matrix which gives rise to local-field corrections. In this paper, the noninteracting-band scheme is extended for bcc transition metals and applied to paramagnetic chromium. The noninteracting-band model is discussed in Sec. II. The calculations and results are given in Sec. III, and the results are discussed in Sec. IV.

### II. MODEL BAND STRUCTURE

Many detailed calculations of the band structure of paramagnetic chromium exist in the literature.<sup>10-12</sup> We use the detailed augmented-plane-wave (APW) calculations of Gupta and Sinha<sup>12</sup> to construct an isotropic-noninteracting-band model because these authors have also calculated the diagonal part of the dielectric matrix. We follow a procedure similar to that adopted in paper I. The  $s$  bands are obtained by joining  $\Gamma_1$  to  $H_1$ ,  $\Gamma_1$  to  $N_1$ , and  $\Gamma_1$  to  $P_1$  in the [100], [110], and [111] directions, respectively. For  $d$  subbands,  $\Gamma_{12}$  is joined to  $H_{12}$  in the [100] direction,  $\Gamma_{25'}$  is joined with lower  $N_1$  point in the [110] direction, and  $\Gamma_{25'}$  is joined to  $P_4$  in the [111] direction. The noninteracting band structure along the three principal symmetry directions is shown in Fig. 1. The plot of  $d$  subbands looks similar to that obtained by Asdente *et al.*<sup>10</sup> using the tight-binding approximation. To make the weighted averaged isotropic energy bands, the energy bands along the  $\Gamma$  to  $G$ ,  $\Gamma$  to  $D$ , and  $\Gamma$  to  $F$  directions are also included. A plot of energy bands along these directions is not available in the conventional band-structure calculations. Therefore, we construct them according to the compatibility relations.<sup>13</sup>  $\Gamma_{12}$  is joined to  $G_1, G_4; D_1, D_2;$  and  $F_3$  along the [310], [221], and [311] directions, respectively.  $\Gamma_{25'}$  is joined with  $G_1, G_2, G_3; D_3, D_4, D_1;$  and with  $F_1, F_3$  along the above off-symmetry directions, respectively. The joining between the two points is done through the parabolic-band approximation using the eigenvalues tabulated by Gupta and Sinha. This parabolic band structure is shown in Fig. 2.

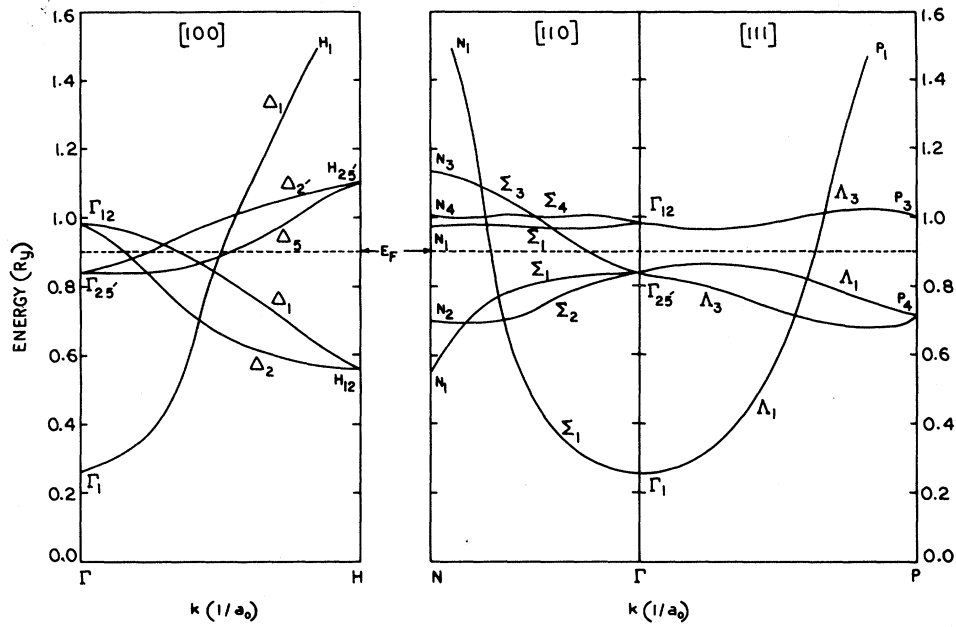


FIG. 1. Noninteracting band model along the three principal symmetry directions [100], [110], and [111] for paramagnetic chromium. The dashed line shows the Fermi energy.

It is evident from Fig. 1 that the *s* band is partially filled, while some of the *d* subbands are partially filled, some are completely filled, and some are completely empty along the different symmetry directions. It is too lengthy to calculate the contribution to the dielectric matrix along

different symmetry directions separately. Therefore, we construct the isotropic-energy-band structure. This requires the assignment of a magnetic quantum number *m* to different *d* subbands. If we completely neglect hybridization and choose the direction of  $\vec{k}$  as the axis of quantization, then

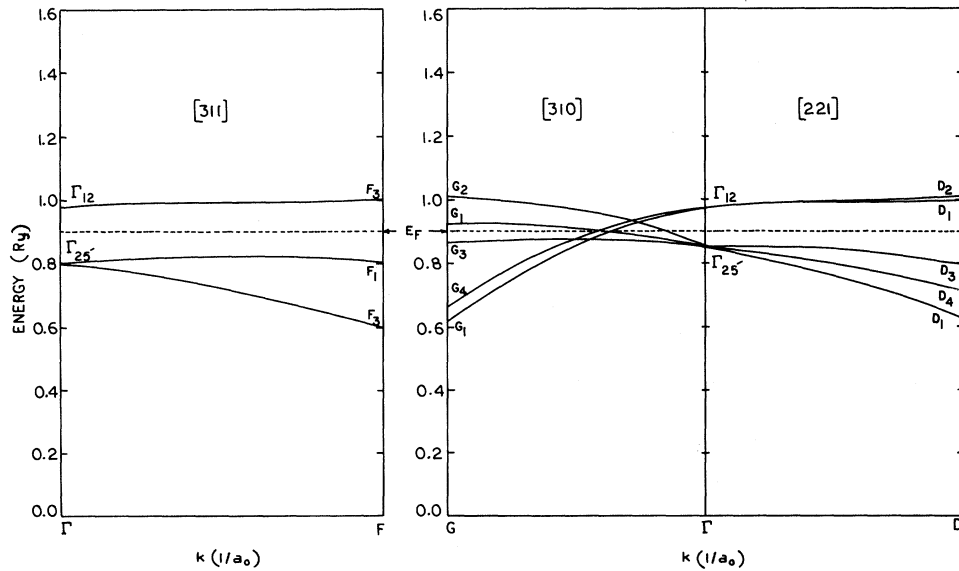


FIG. 2. Noninteracting band model along the three off-symmetry directions [310], [221], and [311] for paramagnetic chromium. The dashed line shows the Fermi energy.

the different  $d$  subbands with  $m=0, \pm 1, \pm 2$  will be in ascending order of energy, and the lowest one will hybridize with the  $s$  band. However, in the detailed APW calculations, the  $s$ - $d$  hybridization and the overlapping of the atomic orbitals is taken into consideration; therefore, such an ordering is not maintained in the noninteracting-band model constructed on the basis of eigenvalues obtained from the detailed band-structure calculations. Hence we assign a magnetic quantum number  $m$  to different  $d$  subbands by examining the  $d$  component of the basis functions of the representations  $\Gamma$ ,  $P$ ,  $H$ ,  $G$ ,  $N$ ,  $D$ , and  $F$ , and assume that to be valid throughout the Brillouin zone.<sup>14</sup>

The  $d$  components of the basis functions of the representations  $\Gamma_{12}$  and  $H_{12}$  are  $Y_2^0$  and  $Y_2^2$ , but the representation  $\Delta_2$  has only one  $d$  component,  $Y_2^2$ . Therefore, the subband obtained by joining  $\Gamma_{12}$  to  $H_{12}$  through  $\Delta_2$  is assigned with magnetic quantum number  $m=2$ , and the band obtained by joining  $\Gamma_{12}$  to  $H_{12}$  through  $\Delta_1$  is assigned  $m=0$ .  $\Gamma_{25'}$  and  $H_{25'}$  have the  $d$  components  $Y_2^1$ ,  $Y_2^{-1}$ , and  $Y_2^{-2}$ , but  $\Delta_2$  has only one component,  $Y_2^{-2}$ ; therefore, the subband  $\Gamma_{25'}$  to  $H_{25'}$  through  $\Delta_2$  is assigned  $m=-2$ , and the remaining band through  $\Delta_5$  is doubly degenerate and is assigned  $m=\pm 1$ . Similarly, in the [110] direction, the upper band from  $\Gamma_{12}$  to  $N_4$  is assigned  $m=0$ , and the lower band  $\Gamma_{12}$  to  $N_1$  is assigned  $m=2$ . The representations  $\Gamma_{25'}$ ,  $N_1$ , and  $\Sigma_1$  have only one common  $d$  component,  $Y_2^{-1}$ ; therefore, the band  $\Gamma_{25'}$  to  $N_1$  through  $\Sigma_1$  is assigned  $m=-1$ . The band obtained by joining  $\Gamma_{25'}$  to  $N_3$  through  $\Sigma_3$  in the [110] direction is assigned  $m=-2$  and, the last band from  $\Gamma_{25'}$  to  $N_2$  through  $\Sigma_2$  is assigned  $m=1$ , according to the splitting of the bands in the [100] direction. The band  $\Gamma_{12}$  to  $P_3$  is doubly degenerate with  $m=0, 2$  in the [111] direction. In order to keep the same ordering of the splitted bands, we assign  $m=-2$  to the band  $\Gamma_{25'}$  to  $P_4$  through  $\Lambda_1$  and  $m=\pm 1$  to the band  $\Gamma_{25'}$  to  $P_4$  through  $\Lambda_3$ , which is doubly degenerate.

In the off-symmetry directions, the  $m$  assignment is made using compatibility relations, and the diagrammatic plots of energy bands of Gupta and Sinha<sup>12</sup> and of Asdente *et al.*<sup>10</sup> The band  $H_{12}$  to  $P_4$  through  $F_3$  joins to the band  $P_4$  to  $\Gamma_{25'}$  through  $\Lambda_3$  which is doubly degenerate and is assigned  $m=\pm 1$ . Therefore, the band  $\Gamma_{25'}$  to  $F_3$  is assigned  $m=\pm 1$ . The band  $\Gamma_{25'}$  to  $F_1$  is assigned  $m=-2$ . The band  $\Gamma_{12}$  to  $F_3$  is doubly degenerate and is assigned  $m=0, 2$  as it joins to the band  $\Gamma_{12}$  to  $P_3$  through  $\Lambda_3$  having the same  $m$  values. According to the splitting of bands in the principal symmetry directions, the band  $\Gamma_{12}$  to  $D_2$  is assigned with  $m=0$ , and the band  $\Gamma_{12}$  to  $D_1$  is assigned with  $m=2$  in the [221] direction. The representations  $P_4$ ,

TABLE I(a). Assignment of magnetic quantum number  $m$  to different  $d$  subbands along the principal symmetry directions.

[100]	[110]	[111]	$m$
$\Gamma_{12} \rightarrow \Delta_1 \rightarrow H_{12}$	$\Gamma_{12} \rightarrow \Sigma_4 \rightarrow N_4$	$\Gamma_{12} \rightarrow \Lambda_3 \rightarrow P_3$	0
$\Gamma_{25'} \rightarrow \Delta_5 \rightarrow H_{25'}$	$\Gamma_{25'} \rightarrow \Sigma_2 \rightarrow N_2$	$\Gamma_{25'} \rightarrow \Lambda_3 \rightarrow P_4$	1
$\Gamma_{25'} \rightarrow \Delta_5 \rightarrow H_{25'}$	$\Gamma_{25'} \rightarrow \Sigma_1 \rightarrow N_1$	$\Gamma_{25'} \rightarrow \Lambda_3 \rightarrow P_4$	-1
$\Gamma_{12} \rightarrow \Delta_2 \rightarrow H_{12}$	$\Gamma_{12} \rightarrow \Sigma_1 \rightarrow N_1$	$\Gamma_{12} \rightarrow \Lambda_3 \rightarrow P_3$	2
$\Gamma_{25'} \rightarrow \Delta_2 \rightarrow H_{25'}$	$\Gamma_{25'} \rightarrow \Sigma_3 \rightarrow N_3$	$\Gamma_{25'} \rightarrow \Lambda_1 \rightarrow P_4$	-2

$D_1$ , and  $N_1$  have only one  $d$  component,  $Y_2^{-1}$ , in common, therefore the band  $\Gamma_{25'}$  to  $D_1$  which also joins to  $P_4$  is assigned  $m=-1$ . The representations  $P_4$ ,  $D_1$ , and  $N_1$  have only one component in common,  $Y_2^{-1}$ ; therefore, the band  $\Gamma_{25'}$  to  $D_1$  which joins with  $P_4$  and  $N_1$  is assigned  $m=1$ . The last band  $\Gamma_{25'}$  to  $D_4$  is assigned the value  $m=-2$ . The band  $H_{25'}$  to  $N_3$  through  $G_2$  is assigned  $m=-2$  because the band  $\Gamma_{25'}$  to  $N_3$  to which it joins is assigned  $m=-2$ . Similarly, the bands  $H_{25'}$  to  $N_2$  through  $G_3$  and  $H_{12}$  to  $N_4$  through  $G_4$  are assigned  $m=1$  and  $m=0$  values, respectively. Therefore, the bands  $\Gamma_{25'}$  to  $G_2$ ,  $\Gamma_{25'}$  to  $G_3$ , and  $\Gamma_{12}$  to  $G_4$  are assigned  $m=-2, 1, 0$ , respectively. The band from  $\Gamma_{25'}$  to  $N_1$  which also joins  $G_1$  is assigned  $m=-1$ , and therefore, the band  $\Gamma_{25'}$  to  $G_1$  (upper point) is assigned  $m=-1$ . The last band in this direction,  $\Gamma_{12}$  to  $G_1$ , is assigned  $m=2$ . The  $m$  assignment to different  $d$  subbands in different directions is shown in Table I.

To construct the isotropic energy-band structure, we first calculate the effective masses for the  $d$  subbands along all the six directions using the energy eigenvalues tabulated by Gupta and Sinha.<sup>12</sup> Using these effective masses, we calculate the corresponding eigenvalues at  $k=\gamma_B$  where  $\gamma_B$  is the radius of the sphere whose volume is equal to the volume of the Brillouin zone. These eigenvalues are averaged using Houston's six-directional-average formula.<sup>15</sup> The averaged energy eigenvalues are then used to calculate the

TABLE I(b). Assignment of magnetic quantum number  $m$  to different  $d$  subbands along [310], [221], and [311] off-symmetry directions.

[310]	[221]	[311]	$m$
$\Gamma_{12} \rightarrow G_4$	$\Gamma_{12} \rightarrow D_2$	$\Gamma_{12} \rightarrow F_3$	0
$\Gamma_{25'} \rightarrow G_3$	$\Gamma_{25'} \rightarrow D_3$	$\Gamma_{25'} \rightarrow F_3$	1
$\Gamma_{25'} \rightarrow G_1$	$\Gamma_{25'} \rightarrow D_1$	$\Gamma_{25'} \rightarrow F_3$	-1
$\Gamma_{12} \rightarrow G_1$	$\Gamma_{12} \rightarrow D_1$	$\Gamma_{12} \rightarrow F_3$	2
$\Gamma_{25'} \rightarrow G_2$	$\Gamma_{25'} \rightarrow D_4$	$\Gamma_{25'} \rightarrow F_1$	-2

effective masses and with the help of these effective masses, an isotropic-energy-band structure is constructed which is shown in Fig. 3. Since there will be much hybridization between different  $m$  components in the isotropic- $d$ -band model, we cannot assign a particular  $m$  value to a particular  $d$  subband. We count the  $d$  subbands from 1 to 5 starting from the lowest  $d$  subband.

The physical parameters and the effective masses for all the five  $d$  subbands are tabulated in Tables II(a) and II(b), respectively. We find in Fig. 3 that the bandwidth for the  $d$  subbands is of the same order of magnitude as the average bandwidth found in the calculations of Gupta and Sinha.

In this paper, the calculations are done for the configuration  $3d^54s^1$  of chromium. Therefore, one electron per atom is assigned to the  $s$  band. It is evident from Fig. 3 that three  $d$  subbands are partially filled and two  $d$  subbands are completely filled. Each filled  $d$  subband is assigned two electrons per atom, and the remaining one electron is distributed among the partially filled  $d$  subbands in the ratio of the volumes occupied by them. The charge distribution of the  $d$  subbands is also given in Table II(b).

### III. DIELECTRIC FUNCTION AND LOCAL-FIELD CORRECTIONS

According to Fig. 3, the following possible transitions will take place:

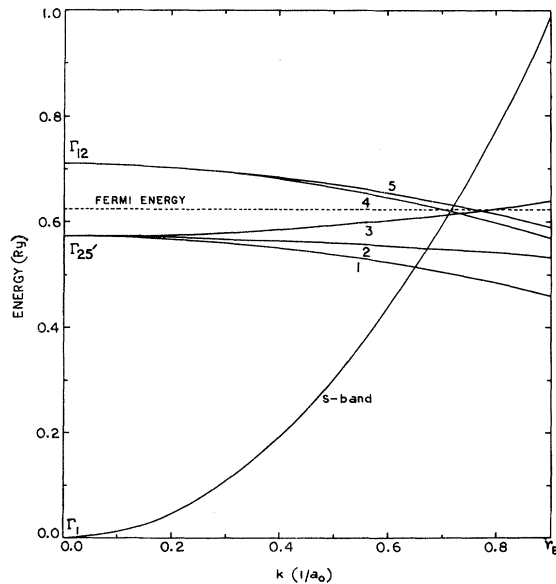


FIG. 3. Isotropic-noninteracting-band model for paramagnetic chromium. The dashed line shows the Fermi energy. The five  $d$  subbands are numbered from 1 to 5.

TABLE II(a). Physical parameters for paramagnetic chromium.

Lattice parameter $a_0'$ = 5.4419 (in Bohr units)
Volume of unit cell = 80.578 96 (in units of $a_0^3$ )
Radius of Brillouin sphere $r_B$ = 0.9024 (in units of $1/a_0$ )

- (i) from a partially filled  $s$  band to a partially filled  $s$  band,
- (ii) from filled and partially filled  $d$  subbands to partially filled  $d$  subbands and  $s$  band,
- (iii) from a partially filled  $s$  band to partially filled  $d$  subbands.

To calculate these contributions, we use Eqs. (5), (7), (8), (11), (12), and (15)–(18) of Paper II by removing the spin index  $\sigma$  and multiplying these expressions by a factor of 2 for spin degeneracy. In order to take into account the hybridization between different  $m$  components of the  $d$  subbands, we give equal weight to all the five  $m$  values. Such an averaging has also been done by Brown<sup>16</sup> and Hanke<sup>17</sup> in the calculation of the dielectric matrix for palladium. We use the  $3d$  radial wave function for chromium tabulated by Clementi<sup>18</sup> in the analytical form:

$$R_{3d}(r) = \sum_{i=1}^5 a_i r^2 e^{-\alpha_i r}.$$

The parameters  $a_i$  and  $\alpha_i$  are tabulated in Table III.

The various contributions to the diagonal part of the dielectric function  $\epsilon(\vec{q} + \vec{G})$  where  $\vec{q}$  is along the [001] direction are compared in Table IV.

$\epsilon_{ss}(\vec{q} + \vec{G})$  and  $\epsilon_{dd}(\vec{q} + \vec{G})$ , which arise because of

TABLE II(b). Fermi momenta (in units of  $1/a_0$ ), effective masses, and charge distribution (in units of electronic charge) in the  $s$  and  $d$  subbands of chromium for the configuration  $3d^54s^1$ .

s band			
	$k_{Fs}$	$m_s$	Charge
	0.716 24	0.822 11	1.0
d subbands			
	$k_{Fdi}$	$m_{di}$	Charge
1	0.9024	-7.335 74	2.0
2	0.9024	-20.335 50	2.0
3	0.7104	11.929 50	0.9757
4	0.1889	-5.771 10	0.0183
5	0.1297	-6.718 58	0.0060

TABLE III. Parameters of 3d radial wave function.

$i$	1	2	3	4	5
$a_i$	7.1287	45.3415	40.0003	3.9975	0.1364
$\alpha_i$	3.4700	10.3587	5.2264	2.3442	1.2645

intra  $s$ - and  $d$ -band transitions, have the same sign and decrease smoothly as  $|\vec{q} + \vec{G}|$  increases.  $\epsilon_{ad}(\vec{q} + \vec{G})$  for  $m = m'$  is approximately 10 times larger than  $\epsilon_{ss}(\vec{q} + \vec{G})$ .  $\epsilon_{ad}(\vec{q} + \vec{G})$  for  $m \neq m'$  and  $\epsilon_{as}(\vec{q} + \vec{G})$  have the same sign.  $\epsilon_{as}(\vec{q} + \vec{G})$  decreases smoothly as  $|\vec{q} + \vec{G}|$  increases, while  $\epsilon_{ad}(\vec{q} + \vec{G})$  for  $m \neq m'$  and  $\epsilon_{sd}(\vec{q} + \vec{G})$  show an oscillatory nature. The qualitative behavior of all the contributions to the dielectric function is the same as found in Papers I and II for paramagnetic nickel. From Table IV it is evident that the contribution due to response of  $d$  electrons plays a dominating role.

We also calculated the dielectric function for  $\vec{q}$  lying in the first Brillouin zone along the three principal symmetry directions [100], [110], and [111], but we noted the anisotropy to be small except in the vicinity of  $|\vec{q}| = 0$ . Therefore, in Fig. 4 we plot the results for the total diagonal part of the dielectric function for  $\vec{q}$  along the  $Z$  direction; only in Fig. 4, the total intraband  $[-\epsilon_{ss}(\vec{q} + \vec{G}) - \epsilon_{ad}(\vec{q} + \vec{G})$  for  $m = m'$ ] and interband  $[-\epsilon_{ad}(\vec{q} + \vec{G})|_{m \neq m'} - \epsilon_{as}(\vec{q} + \vec{G}) - \epsilon_{sd}(\vec{q} + \vec{G})]$  contributions are also displayed separately. For small values of  $|\vec{q} + \vec{G}|$  the magnitude of the intraband part is larger than that of the interband part, while the interband part is larger than the interband part for large values of  $|\vec{q} + \vec{G}|$ . The intraband part decreases faster than the interband part. The qualitative behavior is in agreement with the calculations of Gupta and Sinha. The total diagonal dielectric function, obtained by using the results

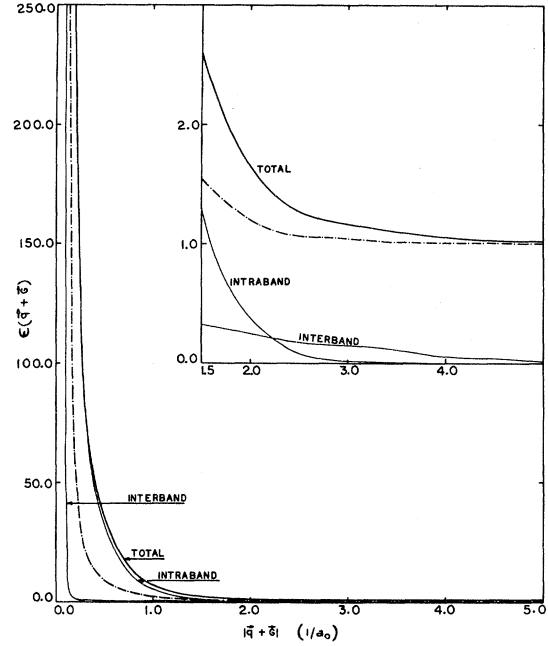


FIG. 4.  $\epsilon(\vec{q} + \vec{G})$  vs  $|\vec{q} + \vec{G}|$  for paramagnetic chromium. The dot-dash line shows the dielectric function obtained from the susceptibility function of Gupta and Sinha (Ref. 12).

of detailed calculations of the susceptibility function of Gupta and Sinha, is also shown in Fig. 4. The dielectric function obtained in our calculations is larger than that due to Gupta and Sinha. This is because the parabolic- $d$ -band approximation overestimates the  $d$ -band contribution.

The nondiagonal part of the dielectric matrix which gives rise to local-field corrections is shown in Fig. 5 where a relative comparison of intraband and interband contributions is also displayed. We find that the magnitude of the intraband part of  $\epsilon_{ad}(\vec{q} + \vec{G}, \vec{q})$  is much larger than the

TABLE IV. Relative magnitudes of  $\epsilon_{ss}$ ,  $\epsilon_{ad}$ ,  $\epsilon_{as}$ , and  $\epsilon_{sd}$ .  $|\vec{q} + \vec{G}|$  is in Bohr units.

$ \vec{q} + \vec{G} $	$\epsilon_{ss}(\vec{q} + \vec{G})$	$\epsilon_{ad}(\vec{q} + \vec{G})$ $m = m'$	$\epsilon_{ad}(\vec{q} + \vec{G})$ $m \neq m'$	$\epsilon_{as}(\vec{q} + \vec{G})$	$\epsilon_{sd}(\vec{q} + \vec{G})$
0.2	-18.6207	-209.9551	-1.0961	-1.1637	0.9922
0.4	-4.5620	-55.2196	-0.0456	-0.4368	0.3966
0.6	-2.3468	-21.8696	-0.0324	-0.1733	0.1650
0.8	-1.0408	-10.1592	-0.0412	-0.0794	0.0924
1.4981	-0.1516	-1.1009	-0.2446	-0.0586	-0.0170
2.5092	-0.0139	-0.0653	-0.1642	-0.0092	-0.0009
2.9937	-0.0067	-0.0161	-0.1382	-0.0036	-0.0003
4.1183	-0.0018	-0.0003	-0.0529	-0.0005	-0.0000
5.0419	-0.0008	-0.0000	-0.0216	-0.0001	-0.0000

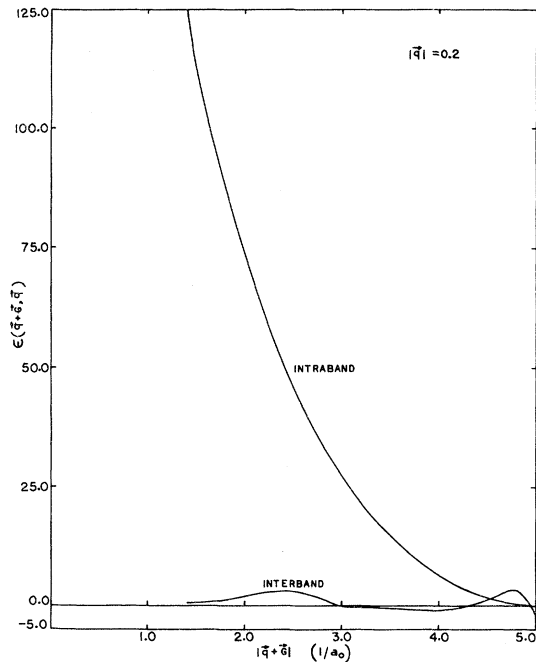


FIG. 5.  $\epsilon(\vec{q} + \vec{G}, \vec{q})$  vs  $|\vec{q} + \vec{G}|$  for  $|\vec{q}| = 0.20$  for paramagnetic chromium.

magnitude of the interband part  $\epsilon_{ad}(\vec{q} + \vec{G}, \vec{q})|_{m \neq m'}$ ,  $\epsilon_{ds}(\vec{q} + \vec{G}, \vec{q})$ , and  $\epsilon_{sd}(\vec{q} + \vec{G}, \vec{q})$  except for very large values of  $|\vec{q} + \vec{G}|$ . On comparison with the corresponding diagonal parts, we find that the local-field corrections are larger for intermediate and large values of  $|\vec{q} + \vec{G}|$  for the intraband part, while they are much smaller for the interband part.

We also calculated the dielectric function including the exchange and correlation corrections factor  $f_{xc}(\vec{q} + \vec{G})$  of Singwi *et al.*,<sup>19</sup> but we applied this correction only for  $\epsilon_{ss}(\vec{q} + \vec{G})$  and  $\epsilon_{sd}(\vec{q} + \vec{G})$  where the  $s$  electrons are itinerant. Such a correction is hardly applicable for  $d$  electrons. These exchange and correlation corrections decrease the result only by less than 5%. Therefore, to simplify the diagram, these are not shown in the figure.

## V. DISCUSSION

We use the plane-wave approximation for  $s$  electrons. In fact, we must use a wave function which is orthogonal to the core as well as to  $d$  wave functions. An orthogonalized plane wave is a suitable choice. However, it has been found that the orthogonalization corrections are very small.<sup>17</sup> The parabolic-band approximation for the energy values is fairly justified for  $s$  electrons, but for tightly bound  $d$  electrons it is crucial. We have constructed the isotropic-noninteracting band model by combining the bands along different symmetry directions according to compatibility relations. The magnetic quantum number  $m$  is assigned on the basis of  $d$  components of the basis functions of high-symmetry points in the Brillouin zone. A point-to-point  $m$  assignment is impracticable in the present scheme. However, in the isotropic- $d$ -band model, these  $m$  components further hybridize. We take into account this hybridization by taking a simple average over all the  $m$  components of the wave function. Overall, a qualitative agreement with the calculations of Sinha *et al.* lends some justification for our model calculation.

In this paper we have calculated the dielectric function and estimated the local-field corrections for chromium in the paramagnetic phase for the first time and concluded that for a bcc transition metal local-field corrections are quite large and should be explicitly accounted for in the calculation of any physical property. An application of this model to the calculation of the phonon frequencies of paramagnetic chromium where Kohn anomalies are present (as in other bcc transition metals) is reported in the subsequent paper.

## ACKNOWLEDGMENTS

The authors are thankful to Professor S. K. Joshi and Professor S. K. Sinha for fruitful discussions. Financial support from the Council of Scientific and Industrial Research, New Delhi, is also acknowledged.

<sup>1</sup>P. Nozières and D. Pines, Phys. Rev. **109**, 741 (1958); *ibid.* **109**, 762 (1958).

<sup>2</sup>H. Ehrenreich and M. H. Cohen, Phys. Rev. **115**, 789 (1959).

<sup>3</sup>S. L. Adler, Phys. Rev. **126**, 413 (1962).

<sup>4</sup>L. J. Sham, Phys. Rev. **188**, 1431 (1959).

<sup>5</sup>E. Hayashi and M. Shimizu, J. Phys. Soc. Jpn. **26**, 1369 (1969); *ibid.* **27**, 43 (1969).

<sup>6</sup>S. Prakash and S. K. Joshi, Phys. Rev. B **2**, 915

(1970).

<sup>7</sup>S. Prakash and S. K. Joshi, Phys. Rev. B **4**, 1770 (1971).

<sup>8</sup>N. Singh and S. Prakash, Phys. Rev. B **8**, 5532 (1973); S. Prakash and S. K. Joshi, Phys. Rev. B **5**, 2880 (1972).

<sup>9</sup>N. Singh, J. Singh, and S. Prakash, Phys. Rev. B **12**, xxx (1975).

<sup>10</sup>M. Asdente and J. Friedel, Phys. Rev. **124**, 384

- (1961).
- <sup>11</sup>M. Yasui, E. Hayashi, and M. Shimizu, *J. Phys. Soc. Jpn.* **29**, 1446 (1970).
- <sup>12</sup>R. P. Gupta and S. K. Sinha, *Phys. Rev. B* **3**, 2401 (1971).
- <sup>13</sup>J. F. Cornwell, *Group Theory and Electronic Energy Bands* (North-Holland, Amsterdam, 1969).
- <sup>14</sup>V. Heine, in *Physics of Metals*, edited by J. M. Ziman, (Cambridge U. P., London, 1969), p. 25.
- <sup>15</sup>D. D. Bett, A. B. Bhatia, and M. Wyman, *Phys. Rev.* **104**, 37 (1965).
- <sup>16</sup>J. S. Brown, *J. Phys. F* **2**, 115 (1972).
- <sup>17</sup>W. R. Hanke, *Phys. Rev. B* **8**, 4583 (1973).
- <sup>18</sup>E. Clementi, *Tables of Atomic Functions*, (San Jose Research Laboratory, San Jose, California).
- <sup>19</sup>K. S. Singwi, A. Sjölander, M. P. Tosi, and R. H. Land, *Phys. Rev. B* **1**, 1044 (1970).